This is a preprint, the final version is subject to change, of the American Mineralogist (MSA)
Cite as Authors (Year) Title. American Mineralogist, in press.
(DOI will not work until issue is live.) DOI: http://dx.doi.org/10.2138/am.2014.4597

Revision 2 with Implications Section

First principles elasticity of monocarboaluminate hydrates

Juhyuk Moon[1], Seyoon Yoon[2], Renata M. Wentzcovitch[3,4], and Paulo J.M. Monteiro[2,*]

[1]Civil Engineering Program, Department of Mechanical Engineering, Stony Brook University, New York 11794, U.S.A.

[2]Department of Civil and Environmental Engineering, University of California, Berkeley, California 94720, U.S.A.

[3]Department of Chemical Engineering and Materials Science, University of Minnesota, Minneapolis, Minnesota 55455, U.S.A.

[4]Minnesota Supercomputing Institute, University of Minnesota, Minneapolis, Minnesota 55455, U.S.A.

* Address: 725 Davis Hall, Department of Civil and Environmental Engineering, University of California, Berkeley CA 94720, U.S.A. Email: monteiro@ce.berkeley.edu

ABSTRACT

The elasticity of monocarboaluminate hydrates, $3CaO{\cdot}Al_2O_3{\cdot}CaCO_3{\cdot}xH_2O$ (x=11 or 8), has been investigated by first-principles calculations. Previous experimental study revealed that

the fully hydrated monocarboaluminate (x=11) exhibits exceptionally low compressibility compared to other reported calcium aluminate hydrates. This stiff hydration product can contribute to the strength of concrete made with portland cements containing calcium carbonates. In this study, full elastic tensors and mechanical properties of the crystal structures with different water contents (x=11 or 8) are computed by first-principles methods based on density functional theory. The results indicate that the compressibility of monocarboaluminate is highly dependent on the water content in the interlayer region. The structure also becomes more isotropic with the addition of water molecules in this region. Since the monocarboaluminate is a key hydration product of limestone added cement, elasticity of the crystal is important to understand its mechanical impact on concrete. Besides, it is put forth that this theoretical calculation will be useful in predicting the elastic properties of other complex cementitous materials and the influence of ion exchange on compressibility.

Keyword: Elasticity, ab initio calculations, Crystal Structure, Monocarboaluminate

INTRODUCTION

Carbonate sources from calcium carbonate, kiln dust, or atmospheric carbon dioxide can form carbon containing AFm (Al_2O_3-Fe_2O_3-mono) phases (Kuzel and Pöllmann, 1991; Lothenbach et al., 2008; Matschei et al., 2007a; Matschei et al., 2007b). Especially in the case of portland-limestone cements (maximum content of limestone is 35%), the presence of carbonate prevents the conversion of monosulfoaluminate from ettringite. Instead of the

monosulfoaluminate, monocarboaluminate and ettringite are stabilized in the presence of the limestone. Thus, these stabilized hydrates decrease the porosity and increase concrete strength (Lothenbach et al., 2008). By maximizing the assemblage of monocarboaluminate and ettringite, it is possible to obtain the best space filling relative to other cement hydrates and, therefore, increase the strength of the cementitious matrix. Recently, Moon et al. reported the bulk modulus of monocarboaluminate (54 GPa) is significantly higher than any other hydration products in concrete (Moon et al., 2012). The unusual mechanical properties of monocarboaluminate can also influence to the structural response of the cementitous matrix.

Two representative carbon containing AFm phases are monocarboaluminate ($C_4A\bar{C}H_{11}$, triclinic, P1 or $P\bar{1}$ system) and hemicarboaluminate ($C_4A\bar{C}_{0.5}H_{12}$, trigonal, $R\bar{3}c$ or R3c system) (Matschei et al., 2007a). Note that cement chemisty notation of C=CaO, A=Al_2O3, $\bar{C}$=CO_2, and H=H_2O is used to simplify chemical notations. Two modifications of monocarboaluminate have been solved as an ordered arrangement with the triclinic P1 symmetry (François et al., 1998) and a disordered arrangement with the triclinic $P\bar{1}$ symmetry (Renaudin et al., 1999) whereas the crystal structure of hemicarboaluminate has not been solved.

The AFm phases have a layered structure where one third of Ca^{2+} ions of portlandite are substituted by Al^{3+} or Fe^{3+}, with the main layer having the chemical formula $[Ca_2(Al,Fe)(OH)_6]^+$. The layer structure $[X_nH_2O]^-$ incorporates variable amounts of water, as well as charge-balancing X anions such as hydroxyl, chloride, carbonate, sulfate, and silicate. The type of the X anion and the amount of interlayer water determines the layer thickness, compressibility, and chemical stability (Taylor, 1973; Taylor, 1997). At ambient condition, a unit cell of monocarboaluminate

contains a CO_3^{2-} group and five water molecules in the interlayer region, with the planar CO_3^{2-} groups tilted by 21.8(9)° with respect to planes of the main calcium aluminum oxide layers (François et al., 1998; Renaudin et al., 1999). Among the five, two water molecules are slightly bonded, but three water molecules and O atoms in the carbonate groups act as cohesion forces between the interlayers (François et al., 1998). Monocarboaluminate with two water molecules and without water molecules in the interlayer region are found at 95°C and 130°C drying conditions, respectively, (Fischer and Kuzel, 1982; Taylor, 1997) but their crystal structures have not been resolved yet.

Synchrotron-based x-ray diffraction data on AFm phases of hemicarboaluminate and strätlingite indicated that dehydration occurs under hydrostatic compression (Moon et al., 2011). This makes the crystal stiffer and yields larger isothermal bulk modulus at pressures above 1.5 GPa. However, this phenomenon is not applicable to monocarboaluminate (Moon et al., 2012). Its bulk modulus (K_0=54 GPa) is almost four times larger than that of hemicarboaluminate (K_0=14 GPa) and this high stiffness seems to prevent dehydration. This can be the one of the reasons of the mechanical strengthening of concrete attained by the use of limestone. Unfortunately, detailed atomic structure of monocarboaluminates could not be refined through the high-pressure experiments because of the extremely small sample size and complexity of the crystal structure. Consequently the detailed atomic structure under high pressure remained undefined, especially the locations of the interlayer water molecules and orientation of anionic carbonate group.

In this study, the crystal structures of two monocarboaluminate hydrates, with 5 interlayer waters (5-water MC) and 2 interlayer waters (2-water MC) have been investigated. We have performed first principles calculations using two different exchange-correlation functionals. Their accuracy for these systems is investigated by comparing results with published experimental crystallographic data and elasticity. The relationship between crystallographic information and structural behavior under pressure has been resolved. From optimized equilibrium structures, full elastic tensors, averaged mechanical properties, and static bulk modulus of both monocarboaluminate hydrates have been computed.

COMPUTATIONAL DETAILS

Density functional theory (Hohenberg and Kohn, 1964; Kohn and Sham, 1965) has been used to address the elasticity of both fully and partially hydrated monocarboaluminate phases. All computations were performed on Linux clusters in the Molecular Graphics and Computation Facility at the University of California, Berkeley. The DFT calculations were performed using LDA and Perdew-Burke-Ernzerhof (PBE) GGA (Perdew et al., 1996) exchange-correlation functionals and plane wave techniques implemented in the Quantum ESPRESSO distribution (Giannozzi and et al., 2009). Ultrasoft-type pseudopotentials (Vanderbilt, 1990) were used with a plane-wave energy cut-off of 1600 eV. The reference valence configurations and core radii for GGA and LDA pseudopotentials were chosen as $3s^2$, $3p^6$, $4s^2$, r_c = 1.2 Å for Ca, $2s^2$, $2p^6$, $3s^2$, $3p^1$, r_c = 1.1 Å for Al, $2s^2$, $2p^4$, r_c = 0.8 Å for O, $2s^2$, $2p^2$, r_c = 0.8 Å for C, and $1s^1$ for H. In addition, a converged **k**-points grid of 4 × 2 × 2 (Monkhorst and Pack, 1976) was used.

Before calculating structural and elastic properties, structural optimizations were performed at arbitrary pressures (Wentzcovitch, 1991). As a starting crystal structure, the ordered monocarboaluminate was used for a 5-water MC (François et al., 1998). Since no atomic information has been reported for a partially hydrated monocarboaluminate, the structure has been created by removing three water molecules from 5-water MC. A previous study demonstrated that water molecules of 16 and 17 have weak hydrogen bonds (François et al., 1998; Moon et al., 2012) (Figure 1). Therefore, the weakly bonded molecules were removed to generate a partially hydrated monocarboaluminate (2-water MC). In addition, a water molecule of oxygen number of 14 was also removed to be consistent with the reported chemical formula of 2-water MC, $C_4A\bar{C}H_8$ (Fischer and Kuzel, 1982; Taylor, 1997). Atomic positions and lattice parameters were optimized until atomic forces were smaller than 10^{-4} eV/Å and total energy converged within 10^{-6} eV. The final residual stress components of the optimized structure were less than 0.1 kbar.

RESULTS

The optimized crystallographic data are compared in Table 1. Lattice parameters from the structure using the GGA functional compare more favorably with single-crystal (François, 1998) and ambient pressure x-ray diffraction data (Moon et al., 2012). All lattice parameters were predicted within 1% error range in GGA calculation. However, LDA underestimates c lattice parameter (3%) and overestimates α lattice parameter (1%). In addition, LDA predicts the tilting angle between the carbonate group and the parallel layers as 9.2°, which is quite

smaller than the GGA angle (18.8°) and the experimental value (21.7°). Detailed crystallographic analysis of the 2-water MC does not exist for comparison. However, the experimentally observed interlayer spacing of 7.2Å is only 1% smaller than the GGA result (7.29Å) but 7% larger than the LDA result (6.68Å). Figure 2 shows experimental and simulated x-ray diffraction patterns for the 5-water MC and the 2-water MC structures. Again, it is confirmed that the x-ray pattern of GGA is closely matched with the experimental pattern of 5-water MC. The simulated x-ray profile of 2-water MC should enable reliable indexing and easier recognition of the partially hydrated monocarboaluminate in concrete systems. In our previous experiment the x-ray pattern is more diffuse than simulated one. This could be due to the disorder of hydrogens or water molecules in real system. This will be discussed in discussion section. The computed hydrogen bonding network and its distributions in the optimized monocarboaluminates are shown in Figures 3 and 4.

Pressure-volume behavior

Static equilibrium structures at arbitrary pressures were obtained at arbitrary pressures using damped variable cell shape molecular dynamics (Wentzcovitch, 1991). Figure 5 shows simulated x-ray diffraction patterns from LDA and GGA structures together with experimental x-ray patterns previously obtained at similar hydrostatic pressures. Energy-volume relations are presented in Figure 6. They clearly show the smaller compressibility (greater curvature) and larger bulk modulus of the 5-water MC structure with respect to those of the 2-water MC structure. As shown in Figure 7, LDA and GGA compression curves for the 5-water MC structure compare well with the experimental data, with the LDA giving a better agreement.

GGA overestimates its volume at ambient pressure. Computed lattice parameters for the same structure at different pressures are shown in Figure 8. The general behaviors of calculated parameters are very similar to the experimental behaviors. It is interesting to note that LDA predicted the c parameter to be 3% smaller but the angle α to be 5% larger, showing a correlation between these parameters. They compensate for each other and produce volumes similar to the experimental volume, i.e., only 1% larger in the pressure range investigated.

Elastic tensor coefficients

Elastic tensor coefficients for these structures have been computed using stress-strain relations. For infinitesimal strains this relation is linear and at 0 GPa it is simply:

$$\sigma_i = \sum_{j=1}^{6} C_{ij}\varepsilon_j \quad (1)$$

After structural optimization at 0 GPa, individual strains were applied to the equilibrium structure, internal structural degrees of freedom were re-optimized, and stresses computed. Residual stress components for these optimized and re-optimized structures were less than 0.1 kbar. This allows computations of elastic coefficients with well constrained and small errors (Nielsen and Martin, 1983). The elastic tensor of a triclinic structure has twenty-one independent constants:

160
$$C_{ij} = \begin{bmatrix} C_{11} & C_{12} & C_{13} & C_{14} & C_{15} & C_{16} \\ & C_{22} & C_{23} & C_{24} & C_{25} & C_{26} \\ & & C_{33} & C_{34} & C_{35} & C_{36} \\ & & & C_{44} & C_{45} & C_{46} \\ & & & & C_{55} & C_{56} \\ sym. & & & & & C_{66} \end{bmatrix} \quad (2)$$

161 These are defined in an orthogonal coordinate system, thus cell parameters are related to a
162 Cartesian coordinate XYZ setting: The $\vec{X} \parallel \vec{a}$, $\vec{Z} \parallel \vec{a} \times \vec{b}$, and $\vec{Y} \parallel \vec{Z} \times \vec{X}$ setting is chosen to
163 define elastic constants. The Lagrangian strains in Cartesian coordinates are:

164
$$\varepsilon_1 = \begin{pmatrix} \delta & 0 & 0 \\ 0 & 0 & 0 \\ 0 & 0 & 0 \end{pmatrix}, \quad \varepsilon_2 = \begin{pmatrix} 0 & 0 & 0 \\ 0 & \delta & 0 \\ 0 & 0 & 0 \end{pmatrix}, \quad \varepsilon_3 = \begin{pmatrix} 0 & 0 & 0 \\ 0 & 0 & 0 \\ 0 & 0 & \delta \end{pmatrix} \quad (3)$$

165
$$\varepsilon_4 = \begin{pmatrix} 0 & 0 & 0 \\ 0 & 0 & \delta/2 \\ 0 & \delta/2 & 0 \end{pmatrix}, \quad \varepsilon_5 = \begin{pmatrix} 0 & 0 & \delta/2 \\ 0 & 0 & 0 \\ \delta/2 & 0 & 0 \end{pmatrix}, \quad \varepsilon_6 = \begin{pmatrix} 0 & \delta/2 & 0 \\ \delta/2 & 0 & 0 \\ 0 & 0 & 0 \end{pmatrix} \quad (4)$$

166 where the indices are given in Voigt notation. Sufficiently small strains of $\delta = \pm 0.5\%$ were
167 applied, and elastic coefficients were obtained by averaging stresses resulting from positive and
168 negative strains. This procedure eliminates non-linear contributions to the stress-strain relation
169 (Wentzcovitch et al., 1995). Table 2 compares the computed LDA and GGA elastic
170 coefficients for 5-water and 2-water MC structures.

171

172 **Bulk modulus**

173 The isothermal bulk modulus is obtained by fitting a finite strain expansion to the
174 calculated free energy versus volume relation. For large compression, it is standard to expand
175 the free energy in terms of a isotropically defined Eulerian strain, *f*:

176 $$f = \frac{1}{2}\left[\left(\frac{V_0}{V}\right)^{2/3} - 1\right] \quad (5)$$

177 where V_0 and V are a reference volume and compressed volume under pressure, respectively.
178 Then the Helmholtz free energy versus volume relation is expanded in a power series in terms of
179 the Eulerian strains. In this static calculation, the Helmholtz free energy, *F*, is the same as the
180 internal energy, E (F=E-TS) since T = 0 K. The Birch-Murnaghan equation of state
181 corresponds to a finite strain expansion to third power in the strain (Birch, 1978). Pressure is
182 then given by:

183 $$P = -\left(\frac{\partial f}{\partial V}\right)\left(\frac{\partial F}{\partial f}\right)_T \quad (6)$$

184 Using the definition of static bulk modulus, $\lim_{\substack{f\to 0 \\ V\to V_0}} -V\left(\frac{\partial P}{\partial V}\right)_T \equiv K_0$, and of its derivative,

185 $\lim_{\substack{f\to 0 \\ V\to V_0}} \frac{\partial K}{\partial P} \equiv K_0'$, gives:

186 $$P = \frac{3}{2}K_0\left\{\left(\frac{V}{V_0}\right)^{-\frac{7}{3}} - \left(\frac{V}{V_0}\right)^{-\frac{5}{3}}\right\}\left[1 + \frac{3}{4}\left(K_0' - 4\right)\left\{\left(\frac{V}{V_0}\right)^{-\frac{2}{3}} - 1\right\}\right] \quad (7)$$

187 This is Birch-Murnaghan equation of state that is used extensively in the literature to fit pressure
188 volume relations. The fitting gives the reference volume, bulk modulus at zero pressure, and its
189 pressure derivative at 0 GPa as summarized in Table 3. In the table we also report a fitting to
190 the Murnaghan equation of state. This equation results from a finite strain expansion of the free
191 energy to second power in strain. It is equivalent to Eq. (7) but with fixed K_0' (=4). Detailed
192 comparisons will be discussed in next.

193

194 **Aggregate properties**

195 In previous section, isothermal bulk modulus was obtained from the fitting of Eq. (7) to
196 single crystal compression data. In this case, pressure (or stress) is considered uniform
197 throughout compressed structures. In this section, bulk modulus corresponds to the
198 compression of an isotropic polycrystalline aggregate is considered. Poly-crystalline averages
199 are difficult to estimate since they involve statistical averages over grain sizes and orientations.
200 But a scheme has been devised to give average values and upper and lower bounds to the bulk
201 modulus, K, and to the shear modulus, G, in terms of the elastic coefficients. This is the Voigt-
202 Reuss-Hill (VRH) (Watt et al., 1976) averaging method. The Voigt moduli correspond to a
203 situation in which the aggregate is subjected to uniform strain. It provides the upper bounds for
204 K and G. The Reuss moduli correspond to the situation of uniform stress and give the lower
205 bounds. The Voigt-Reuss-Hill moduli are the average of Voigt and Reuss moduli and
206 correspond roughly to the situation in which neither stress or strain are uniform (Hill, 1952;
207 Watt, 1976). The bound values were computed using elastic coefficients, C, determined by first

208 principles from Eqn. 2. From the computed K_{VRH} and G_{VRH}, the Young's modulus (E) and
209 Poisson ratio (η) could be also calculated. These bounds are:

210 Voigt bound:

211 $$K_V = \frac{(C_{11} + C_{22} + C_{33}) + 2(C_{12} + C_{23} + C_{31})}{9} \quad (8)$$

212 $$G_V = \frac{(C_{11} + C_{22} + C_{33}) - (C_{12} + C_{23} + C_{31}) + 3(C_{44} + C_{55} + C_{66})}{15} \quad (9)$$

213 Reuss bound:

214 $$K_R = \frac{1}{(S_{11} + S_{22} + S_{33}) + 2(S_{12} + S_{23} + S_{31})} \quad (10)$$

215 $$G_R = \frac{15}{4(S_{11} + S_{22} + S_{33}) - 4(S_{12} + S_{23} + S_{31}) + 4(C_{44} + C_{55} + C_{66})} \quad (11)$$

216 where the compliance tensor, S, is the inverse of the elasticity tensor, $S = C^{-1}$. Averaged
217 mechanical properties are then:

218 $$K_{VRH} = \frac{K_V + K_R}{2} = K \qquad G_{VRH} = \frac{G_V + G_R}{2} = G \qquad (12)$$

219 $$\eta = \frac{(3K - 2G)}{2(3K + G)} \quad E = \frac{9KG}{(3K + G)} \quad (13)$$

220 The computed LDA and GGA properties for 5-water and 2-water MC structures are summarized
221 in Table 3.

Next, the Young's modulus for uniaxial compression along arbitrary directions was computed. The general definition of the directional Young's modulus in terms of unit vectors, $\hat{n}$, along the compression axis is:

$$E_{ani} = \frac{1}{\hat{n}^T \cdot [C^{-1} : (\hat{n} \cdot \hat{n})] \cdot \hat{n}} \quad (14)$$

This expression was used to investigate the anisotropy of monocarboaluminate hydrates reported in Figure 9. Magnitudes of the LDA and GGA Young's modulus for monocarboaluminate hydrates are represented in colors on the surface of sphere with unit radius. The setting of ($\vec{\mathbf{X}} \parallel \vec{\mathbf{a}}$, $\vec{\mathbf{Z}} \parallel \vec{\mathbf{a}} \times \vec{\mathbf{b}}$, and $\vec{\mathbf{Y}} \parallel \vec{\mathbf{Z}} \times \vec{\mathbf{X}}$) was chosen to define X, Y, and Z directions. The large structural anisotropy of monocarboaluminate hydrates is evident. The softest direction of [011] was computed as the direction perpendicular to the principal layer.

DISCUSSION

Although GGA lattice parameters differ by less than 1% from experimental values, the computed unit cell volume is 2% larger (see Table 1). Inclusion of vibrational effects should increase even more this discrepancy. The LDA volume is slightly better, only 1% larger. This better agreement happens despite differences in the structural details, such as smaller c lattice parameter and larger α angles. The GGA and LDA predicted rather different structures for the 2-water MC system. Since there is no reported crystal structure for 2-water MC (except interlayer spacing), the accuracy of the LDA and GGA functionals is addressed by the 5-water

241 MC system. The quality of results depends on the ability of the exchange-correlation functional
242 to mimic many-body electronic interactions in a system. This discrepancy might result from
243 van der Walls dispersion and vibrational effects as these have been disregarded in this static
244 calculation. Note that this is not a strict 0 K calculation because vibrational zero-point energy,
245 E_{ZP}, was not included. Zero-point motion effect has been known to be more important than
246 finite temperature effects (Carrier et al., 2007; Karki et al., 2000; Wentzcovitch et al., 2010).

247 Figures 2 and 5 compare x-ray diffraction patterns of the fully hydrated
248 monocarboaluminates at ambient and under high pressure, respectively. At ambient condition,
249 not only peak positions but also relative peak intensities are well reproduced, especially in the
250 GGA calculations. Experimental diffraction patterns have fewer small peaks, which might
251 suggest some hydrogen or water disorders. In addition, the occurrence of diffused peaks in
252 high-pressure experiment can be from pressure-transmitting medium (silicone oil was used in
253 previous test (Moon et al., 2012) to maintain the crystal in hydrostatic pressure), which can enter
254 into the crystal structure and especially dissipate short-range diffraction peaks. This effect is
255 well known in high-pressure experiments, especially for those crystals with complex layered
256 structures with large interlayer spacing (Moon et al., 2012). Calculations do not consider such
257 pressure-medium effect. The overall, this agreement ensures that the atomic arrangement and
258 structure are well maintained at high pressures as shown in Figure 5.

259 As shown in Figure 7, the LDA and GGA high-pressure behaviors of 5-water MC are
260 similar to that from previous experiments. In general, the expanded GGA volume (~2%) causes
261 underestimation of the bulk modulus. In this study, the discrepancy is rather large producing an

underestimation of ~29% (37.9 GPa versus 54 GPa from experiments). The accuracy of LDA calculations is expected to improve upon introduction of vibrational effects by means of the quasi-harmonic approximation (QHA). Vibrational effects are particularly important in considering the water molecules in the interlayer region.

For hemicarboaluminate —another carbonated AFm phase— opposite high pressure induced behavior was observed, irrespective of the type of pressure-transmitting medium. A contraction in volume and a significant increase on bulk modulus was observed as a result of a pressure-induced dehydration and re-orientation of anionic carbonate group to parallel to the main layer. Although no significant change in behavior in 5-water MC was observed, partial dehydration might occur around 1 GPa (Moon et al., 2012); therefore, the variation of tilting angle of the carbonate group might provide a clue to the anomalous behavior. In this simulation study, the tilting angle varied from 18.8° to 15.0° and 9.2° to 9.1° in GGA and LDA, respectively, while pressure changed 0 to 5 GPa. That indicates the carbonated group of the 5-water MC was slightly re-oriented to the parallel direction to the layers. However, since this angle change was not significant, it can be safely assumed that pressure-induced dehydration has more dominant effect on the anomalous behavior of hemicarboaluminate rather than the tilting of carbonate group.

LDA and GGA elastic coefficients computed by applying infinitesimal strains at 0 GPa display similar trends in the 2-water MC and 5-water MC structures (see Table 3). The coefficient corresponding to the axis with compact atomic arrangement, C_{11}, is mostly larger than longitudinal strains along the Y and Z axes, C_{22} and C_{33}, respectively. This is consistent

with the expectation that layered structures are softer in the direction perpendicular to the layers. In addition, the difference between K_o, the bulk modulus derived by fitting equations of state to the compression curve, and K_{RVH}, the bulk modulus of the isotropic poly-crystalline aggregates, is noticeable, as they represent different properties (Table 4). K_0 and K_0' capture the compressive behavior in a wider pressure range (Stixrude and Lithgow-Bertelloni, 2010). K_0 values from 2nd order finite strain EoS are larger than those from a 3rd order finite strain EoS. This is due to the smaller K_0' values (i.e., 4.0) used in the fitting of the 2nd order EoS. As previously noted, LDA K_0 values using 2nd and 3rd order finite strain EoSs are quite accurate (less than 4% different).

DFT calculations are useful in predicting structural properties for systems where no data exists. Thus, the general trends on crystal structure under pressure for the 2-water MC system (Tables 1-3) can be reliabe. For both LDA and GGA calculations, the 2-water MC system is more compressible, and the cause of this smaller bulk modulus is the smaller number of water molecules in the interlayer region. The larger hydrogen bond-length in the 2-water MC results in a softer structure (Figures 4). The water molecules in the 5-water MC structure are more packed in the interlayer region which makes this structure more incompressible.

Irrespective of the exchange-correlation functional used, the more hydrated the structure the less compressible it becomes. Figure 9 shows highly anisotropic Young's moduli for both the 5- and 2-water MC due to the layered nature of the structures. Less hydrated 2-water MC structure has a wider range of Young's modulus as a function of direction (color bars in Figure 9) and a smaller mechanical properties such as K_{RVH}, G_{RVH}, and E (Table 4). Adding more

304 waters to the 2-water MC structure can notably decrease this anisotropy and increase both bulk
305 moduli from static compression curves and the polycrystalline bulk modulus. The soft elastic
306 coefficient perpendicular to the layers of the 5-water MC system stiffens and becomes more
307 similar to the other longitudinal strain coefficients, which decreases the anisotropy of this layered
308 structure.

309 Elastic constants at high pressures were computed and summarized in Table 3. The
310 identical procedure (Eqs. 1-4) was applied but an optimized structure at high pressure was
311 selected as an unstrained structure. Accordingly, averaged mechanical properties at high
312 pressures could be computed by Eqs. 8-13 and summarized in Tables 4 and 5. In 2-water MC
313 system, the RVH bulk modulus is increased by 56-64% at 5 GPa (GGA: from 27.3 to 44.9 GPa,
314 LDA: from 55.7 to 86.8 GPa). On the other hand, the increment for 5-water MC is 29~53% at 5
315 GPa (GGA: 43.4 to 66.3 GPa, LDA: from 56.2 to 72.9 GPa). This observation suggests the
316 degree of anisotropy can be decreased not only by adding water molecules in interlayers but by
317 increasing overall pressure.

318

319 **IMPLICATIONS**

320 Monocarboluminate is one of the most important crystals in carbonated cement paste.
321 In this study, two monocarboaluminate hydrates were examined by DFT simulation and
322 compared with previously performed high-pressure x-ray experiment. In case of fully hydrated
323 monocarboluaminte, GGA result predicts precise lattice parameters while LDA provides more

accurate mechanical properties. Given the importance of monocarboaluminate for AFm phases, accurate knowledge of elastic properties of this phase is a central ingredient for understanding and modeling concrete. Table 4 compares the compressive properties of calcium aluminate phases. The fully hydrated monocarboaluminate phase has the largest bulk modulus of any other cementitious phases reported so far (Figure 10). Therefore, the bulk modulus and elastic coefficients obtained in this study will be useful to evaluate the mechanical impact of limestone hydration and carbon uptake in concrete system. Further experimental and theoretical studies on other calcium aluminate hydrate phases are being conducted now.

ACKNOWLEDGMENTS

This publication was based on work supported in part by Award No. KUS-l1-004021, made by King Abdullah University of Science and Technology (KAUST). The Advanced Light Source is supported by the Director, Office of Science, Office of Basic Energy Sciences, of the U.S. Department of Energy under Contract No. DE-AC02-05CH11231. RMW was supported by NSF/EAR 1161023. The UC Berkeley Molecular Graphics and Computation Facility is supported by NSF/CHE-0840505.

REFERENCES CITED

Birch, F. (1978) Finite strain isotherm and velocities for single-crystal and Polycrystalline NaCl at high pressures and 300K. Journal of Geophysical Research, 83(B3), 1257-1268.

Carrier, P., Wentzcovitch, R., and Tsuchiya, J. (2007) First-principles prediction of crystal structures at high temperatures using the quasiharmonic approximation. Physical Review B, 76(6), 064116.

346 Clark, S.M., Colas, B., Kunz, M., Speziale, S., and Monteiro, P.J.M. (2008) Effect of pressure on the
347 crystal structure of ettringite. Cement and Concrete Research, 38(1), 19-26.
348 Fischer, R., and Kuzel, H.J. (1982) Reinvestigation of the system $C_4A.nH_2O$-$C_4A.CO_2.nH_2O$. Cement and
349 Concrete Research, 12(4), 517-526.
350 François, M., Renaudin, G., and Evrard, O. (1998) A Cementitious Compound with Composition
351 $3CaO.Al_2O_3.CaCO_3.11H_2O$. Acta Crystallographica Section C, 54(9), 1214-1217.
352 Giannozzi, R., and et al. (2009) QUANTUM ESPRESSO: a modular and open-source software project
353 for quantum simulations of materials. Journal of Physics: Condensed Matter, 21(39), 395502.
354 Hill, R. (1952) The Elastic Behaviour of a Crystalline Aggregate. Proceedings of the Physical Society.
355 Section A, 65(5).
356 Hohenberg, P., and Kohn, W. (1964) Inhomogeneous electron gas. Physical Review, 136(3B), B864.
357 Karki, B.B., Wentzcovitch, R.M., de Gironcoli, S., and Baroni, S. (2000) High-pressure lattice dynamics
358 and thermoelasticity of MgO. Physical Review B, 61(13), 8793.
359 Kohn, W., and Sham, L.J. (1965) Self-consistent equations including exchange and correlation effects.
360 Physical Review, 140(4A), A1133.
361 Kuzel, H.J., and Pöllmann, H. (1991) Hydration of C_3A in the presence of $Ca(OH)_2$, $CaSO_4{\cdot}2H_2O$ and
362 $CaCO_3$. Cement and Concrete Research, 21(5), 885-895.
363 Lothenbach, B., Le Saout, G., Gallucci, E., and Scrivener, K. (2008) Influence of limestone on the
364 hydration of Portland cements. Cement and Concrete Research, 38(6), 848-860.
365 Matschei, T., Lothenbach, B., and Glasser, F.P. (2007a) The AFm phase in Portland cement. Cement and
366 Concrete Research, 37(2), 118-130.
367 Matschei, T., Lothenbach, B., and Glasser, F.P. (2007b) The role of calcium carbonate in cement
368 hydration. Cement and Concrete Research, 37(4), 551-558.
369 Matthies, S., and Wenk, H.R. (2009) Transformations for monoclinic crystal symmetry in texture
370 analysis. Journal of Applied Crystallography, 42(4), 564-571.
371 Meade, C., and Jeanloz, R. (1990) Static compression of Ca (OH) 2 at room temperature: observations of
372 amorphization and equation of state measurements to 10.7 GPa. Geophysical Research Letters,
373 17(8), 1157-1160.
374 Monkhorst, H.J., and Pack, J.D. (1976) Special points for Brillouin-zone integrations. Physical Review B,
375 13(12), 5188-5192.
376 Moon, J., Oh, J.E., Balonis, M., Glasser, F.P., Clark, S.M., and Monteiro, P.J.M. (2011) Pressure induced
377 reactions amongst calcium aluminate hydrate phases. Cement and Concrete Research, 41(6), 571-
378 578.
379 Moon, J., Oh, J.E., Balonis, M., Glasser, F.P., Clark, S.M., and Monteiro, P.J.M. (2012) High Pressure
380 Study of Low Compressibility Tetracalcium Aluminum Carbonate Hydrates
381 $3CaO.Al_2O_3.CaCO_3.11H_2O$. Cement and Concrete Research, 42(1), 105-110.
382 Nielsen, O.H., and Martin, R.M. (1983) First-Principles Calculation of Stress. Physical Review Letters,
383 50, 697-700.
384 Oh, J.E., Clark, S.M., and Monteiro, P.J.M. (2011) Does the Al substitution in C-S-H (I) change its
385 mechanical property? Cement and Concrete Research, 41(1), 102-106.
386 Oh, J.E., Clark, S.M., Wenk, H.R., and Monteiro, P.J.M. (2012) Experimental determination of bulk
387 modulus of 14Å tobermorite using high pressure synchrotron X-ray diffraction. Cement and
388 Concrete Research, 42(2), 397-403.
389 Perdew, J.P., Burke, K., and Ernzerhof, M. (1996) Generalized Gradient Approximation Made Simple.
390 Physical Review Letters, 77(18), 3865-3868.
391 Renaudin, G., Francçis, M., and Evrard, O. (1999) Order and disorder in the lamellar hydrated
392 tetracalcium monocarboaluminate compound. Cement and Concrete Research, 29(1), 63-69.

Stixrude, L., and Lithgow-Bertelloni, C (2010) Thermodynamics of the Earth's mantle. Reviews in Mineralogy and Geochemistry, 71, 465-484.

Taylor, H.F.W. (1973) Crystal structures of some double hydroxide minerals. Mineralogical Magazine, 39(304), 377-389.

Taylor, H.F.W. (1997) Cement Chemistry 2nd edition. Thomas Telford, London.

Vanderbilt, D. (1990) Soft self-consistent pseudopotentials in a generalized eigenvalue formalism. Physical Review B, 41(11), 7892.

Wentzcovitch, R.M. (1991) Invariant molecular-dynamics approach to structural phase transitions. Physical Review B, 44(5), 2358.

Watt, J.P., Davies, G.F., and O'Connell, R.J. (1976) The elastic properties of composite materials. Reviews of Geophysics, 14(4), 541-563.

Wentzcovitch, R.M., Ross, N.L., and Price, G. (1995) Ab initio study of $MgSiO_3$ and $CaSiO_3$ perovskites at lower-mantle pressures. Physics of the Earth and Planetary Interiors, 90(1), 101-112.

Wentzcovitch, R.M., Yu, Y.G., and Wu, Z. (2010) Thermodynamic properties and phase relations in mantle minerals investigated by first priniciples quasiharmonic theory. Reviews in Mineralogy & Geochemistry, 71, 59-98.

LIST OF FIGURE CAPTIONS

FIGURE 1. Crystal structures of 5 water monocarboaluminate hydrates projected along [100]. Large blue, small blue, red, black, and brown spheres represent Al, Ca, O, H, and C atoms, respectively.

FIGURE 2. Simulated x-ray diffraction patterns of optimized monocarboaluminates and the reported crystal structure from single-crystal x-ray experiment (François et al., 1998).

FIGURE 3. Geometrically optimized 5 water (**left**) and 2 water (**right**) monocarboaluminate projected along [100]. Same graphical notation in Fig. 1 is used except H atoms in water and hydroxide (denoted as black sticks). The relaxed size of a unit-cell volume of 2-water MC is smaller than that of 5-water MC.

FIGURE 4. Hydrogen bond length distributions of monocarboaluminates obtained in calculations using GGA (**left**) and LDA (**right**).

FIGURE 5. Comparison of x-ray diffraction patterns of the fully hydrated monocarboaluminate at high pressure. The experimental patterns are from presivous high-pressure experiments (Moon et al., 2012). Water disorder and pressure-transmitting solution used in the experiment makes experimental x-ray diffraction more diffuse.

FIGURE 6. LDA energy-volume relations. The 5-water molecule monocarbolaluminate structure is visibly more compressible (smaller bulk modulus) than the 2-water molecule structure.

FIGURE 7. LDA and GGA Compression curves for the 5-water MC structure obtained in this study compared to previous high-pressure data (Moon et al., 2012).

FIGURE 8. Computed axial (**left**) and angular (**right**) compressibilities of 5 water monocarboaluminate comprared to high-pressure experiments (Moon et al., 2012).

FIGURE 9. Directional Young's modulus of monocarboaluminates for 5-water MC using (**a**) GGA and (**b**) LDA functionals and for 2-water MC using (**c**) GGA and (**d**) LDA functionals. Anisotropy decreases by addition of water molecules in the interlayer region.

FIGURE 10. The bulk moduli of major hydration materials in cement paste. The data were obtained from high-pressure experiments using a 2nd order finite strain equation of state (Clark et al., 2008; Meade and Jeanloz, 1990; Moon et al., 2012; Moon et al., 2011; Oh et al., 2011; Oh et al., 2012).

TABLES

TABLE 1. Structural parameters obtained by first principles for fully hydrated monocarboaluminate. Carbonate group angle is the angle between the carbonate group and the principal layer.

	$C_4A\bar{C}H_{11}$							
	GGA	LDA	Exp. (François et al., 1998)	Exp. (Moon et al., 2012)	GGA	LDA	GGA	LDA
P (GPa)	0.0		Ambient		2.0		5.0	
a (Å)	5.829	5.871	5.775(1)	5.77(2)	5.759	5.815	5.667	5.744
b (Å)	8.534	8.463	8.469(1)	8.47(5)	8.363	8.369	8.217	8.305
c (Å)	9.982	9.631	9.923(3)	9.93(4)	9.673	9.463	9.423	9.355
α (°)	65.14	67.89	64.77(2)	64.6(2)	66.30	68.42	66.97	67.97
β (°)	82.32	81.85	82.75(2)	82.8(3)	82.06	81.71	82.07	81.67
γ (°)	80.80	80.91	81.43(2)	81.4(4)	80.75	80.77	80.95	81.08
V (Å^3)	443.5	436.0	433.0(2)	433(3)	419.7	420.9	397.3	406.8
Interlayer Spacing (Å)	7.70	7.44	7.55	7.59	7.46	7.32	7.28	7.27
Carbonate group angle (°)	18.8	9.2	21.7	-	16.0	9.2	15.0	9.1

Note: Standard deviations in parentheses.

TABLE 2. Structural parameters obtained by first principles for partially hydrated monocarboaluminate.

	$C_4A\bar{C}H_8$						
	GGA	LDA	Exp. (Fischer and Kuzel, 1982)	GGA	LDA	GGA	LDA
P (GPa)	0.0		Ambient	2.0		5.0	
a (Å)	5.822	5.7277	-	5.737	5.683	5.620	5.587
b (Å)	8.284	7.820	-	8.002	7.541	7.692	7.458
c (Å)	9.495	8.897	-	9.669	9.684	9.129	9.562
α (°)	68.11	72.77	-	67.43	63.18	68.96	63.59
β (°)	83.13	85.77	-	80.57	73.59	82.94	73.79
γ (°)	81.38	81.65	-	78.30	75.34	81.66	74.87
V ($Å^3$)	419.1	376.4	-	399.6	351.4	363.4	338.3
Interlayer Spacing (Å)	7.29	6.68	7.20	7.21	7.08	6.83	6.99
Carbonate group angle (°)	19.1	11.3	-	22.2	4.7	11.6	3.6

TABLE 3. Calculated elastic coefficients at different pressure (0, 2, and 5 GPa) for fully and partially hydrated monocarboaluminates.

	$C_4A\bar{C}H_{11}$						$C_4A\bar{C}H_8$					
	GGA			LDA			GGA			LDA		
P (GPa)	0.0	2.0	5.0	0.0	2.0	5.0	0.0	2.0	5.0	0.0	2.0	5.0
c11	108.7	102.4	122.9	**96.2**	98.9	101.8	82.2	94.5	102.7	98.9	94.1	121.6
c12	22.9	27.5	39.1	**34.9**	56.3	54.1	13.7	24.2	1.4	42.1	50.3	62.5
c13	32.8	36.2	51.8	**38.2**	44.5	56.5	20.5	29.0	40.0	34.5	61.2	71.9
c14	-7.0	-8.6	-10.1	**-6.8**	-4.7	-4.4	-11.5	-12.1	-10.0	-2.6	-12.8	-11.2
c15	10.1	8.1	10.0	**9.0**	10.2	10.0	7.0	7.6	2.2	7.7	2.3	0.1
c16	4.9	6.0	6.1	**4.1**	7.2	8.0	3.6	7.0	2.3	3.8	5.3	16.0
c22	60.6	79.7	99.4	**81.1**	68.7	104.0	39.9	55.2	38.2	84.6	94.1	123.3
c23	19.7	30.7	44.7	**43.6**	49.0	65.1	21.1	36.9	34.4	45.6	71.8	74.4
c24	3.3	7.6	8.7	**0.8**	8.4	9.7	-7.7	3.8	5.9	6.1	8.5	11.2
c25	3.1	-4.3	-3.3	**-1.2**	0.6	-1.3	1.4	-2.6	24.5	5.8	3.5	0.3

c26	-5.1	-4.8	-5.2	**-6.4**	-4.8	-4.7	-4.4	4.6	-29.5	4.6	0.8	5.4
c33	89.4	87.5	107.9	**100.3**	93.2	100.4	49.4	67.5	67.2	81.0	113.6	138.1
c34	-10.9	-12.2	-9.4	**-2.8**	-4.3	-0.8	-16.5	-16.5	-10.6	-12.4	-23.0	-23.0
c35	-2.3	-6.2	-6.5	**-2.3**	-3.4	-6.5	-0.4	0.8	-6.2	1.9	-6.9	-4.0
c36	-1.2	-2.0	-3.0	**-2.8**	-4.2	-3.1	-1.9	2.0	6.9	1.1	12.6	7.4
c44	37.9	43.8	51.2	**29.4**	34.7	31.4	22.8	35.5	36.2	41.0	34.7	45.5
c45	-0.2	-2.4	-3.7	**-2.5**	-4.0	-3.1	-0.4	-4.1	-2.1	1.1	2.6	4.0
c46	1.1	0.4	-0.5	**-1.7**	-0.7	2.2	1.1	0.4	1.4	4.2	-0.2	-3.6
c55	35.9	50.6	56.9	**33.9**	32.7	31.7	21.9	27.7	32.8	40.7	32.0	37.9
c56	-0.1	0.8	-0.2	**-2.4**	-1.7	-2.9	-1.6	-7.1	-7.6	2.5	-3.6	-10.3
c66	40.4	44.1	48.5	**41.7**	29.7	17.3	37.9	17.4	12.6	30.5	11.2	40.3

Note: Most reliable results are in bold.

TABLE 4. Calculated elastic properties of fully hydrated monocarboaluminate.

		$C_4A\bar{C}H_{11}$						
		GGA	LDA	Exp. (Moon et al., 2012)	GGA	LDA	GGA	LDA
	P (GPa)	0.0		Ambient	2.0		5.0	
3rd finite strain EoS	V_0	443.5	**436.0**	433(2)	419.7	420.9	397.3	406.8
	K_0'	6.5	**4.2**	5.02	-	-	-	-
	K_0	34.5	**55.9**	53(5)	-	-	-	-
2nd finite strain EoS	V_0	443.5	**436.0**	433(2)	419.7	420.9	397.3	406.8
	K_0	37.9	**56.2**	54(4)	-	-	-	-
RVH approximation	K_{RVH}	43.4	**56.2**	-	50.4	61.3	66.3	72.9
	G_{RVH}	33.7	**30.5**	-	37.0	22.9	41.8	22.2
	E	80.3	**77.6**	-	89.2	61.1	103.6	60.4
	η	0.2	**0.3**	-	0.2	0.3	0.2	0.4

Note: Most reliable results are in bold. Standard deviations in parentheses.

TABLE 5. Calculated elastic properties of partially hydrated monocarboaluminate

		$C_4A\bar{C}H_8$					
		GGA	LDA	GGA	LDA	GGA	LDA
	P (GPa)	0.0		2.0		5.0	
3rd finite strain EoS	V_0	419.1	376.4	399.6	351.4	363.4	338.3

	K_0'	5.88	6.8	-	-	-	-
	K_0	20.7	48.2	-	-	-	-
2^{nd} finite strain EoS	V_0	419.1	376.4	399.6	351.4	363.4	338.3
	K_0	23.8	52.5	-	-	-	-
RVH approximation	K_{RVH}	27.3	55.7	42.3	70.2	44.9	86.8
	G_{RVH}	21.5	29.6	20.8	17.1	31.4	33.1
	E	51.1	75.5	53.6	47.4	76.3	88.1
	η	0.2	0.3	0.3	0.4	0.2	0.3

458

459

460
461 **TABLE 6.** Comparison of bulk modulus and its pressure derivative for calcium
462 aluminate phases

	Method	Pressure range (GPa)	V_0 (Å^3)	K_o'	3rd finite strain EoS, K_o (GPa)	2nd finite strain EoS, K_o (GPa)	Ref.
Monocarboaluminate $C_4A\bar{C}H_X$ (x=11 or 8)	HPXRD (SO, x=11)	0.1-4.3	433(2)	5.02	53(5)	54(4)	(Moon et al., 2012)
	DFT-LDA (x=11)	0-5.0	436.0	4.2	55.9	56.2	This study
	DFT-LDA (x=8)	0-5.0	376.4	6.8	48.2	52.5	
Hemicarboaluminate $C_4A\bar{C}_{0.5}H_{12}$	HPXRD (SO)	0.1-1.1	1418.04(1)	n.d	n.d	15(2)	(Moon et al., 2011)
	HPXRD (ME)	0.1-1.8	1418.94(4)	13.6	9(2)	14(1)	
Strätlingite C_2ASH_8	HPXRD (SO)	0.1-1.5	1077.30(2)	n.d.	n.d.	23(2)	(Moon et al., 2011)
Ettringite $C_6A\bar{S}_3H_{32}$	HPXRD (SO)	0.1-1.2	2352.8(1)	-	-	27(7)	(Clark et al., 2008)

463 Notes: n.d: not determined, (ME) and (SO) indicate, respectively, the methanol:ethanol
464 = 4:1 solution, and silicone oil. Standard deviations in parentheses.

465
466

467
468 **SUPPLEMENTARY TABLE 1.** Selected geometric parameters (Å, °).

	$C_4AC̄H_{11}$							$C_4AC̄H_8$					
	Exp.	LDA			GGA			LDA			GGA		
P (GPa)	0.0	0.0	2.0	5.0	0.0	2.0	5.0	0.0	2.0	5.0	0.0	2.0	5.0
Ca1-O10	2.350 (3)	2.549	2.538	2.527	2.353	2.334	2.312	2.669	2.634	2.622	2.337	2.314	2.327
Ca1-O5	2.351 (3)	2.543	2.530	2.520	2.362	2.339	2.311	2.575	2.893	2.837	2.351	2.311	2.332
Ca1-O3^{i}	2.359 (3)	2.563	2.545	2.528	2.369	2.345	2.314	2.939	2.594	2.589	2.398	2.316	2.369
Ca1-O4^{ii}	2.445 (3)	2.590	2.577	2.570	2.459	2.440	2.410	2.690	2.581	2.562	2.463	2.374	2.365
Ca1-O10	2.455 (2)	2.627	2.614	2.602	2.480	2.467	2.454	2.512	2.806	2.775	2.489	2.324	2.435
Ca1-O12	2.457 (2)	2.654	2.608	2.580	2.500	2.469	2.430	3.216	2.752	2.731	2.510	2.452	2.493
Ca1-O13^{i}	2.546 (3)	2.672	2.638	2.616	2.590	2.603	2.573	2.602	2.631	2.607	2.591	4.593	2.416
Ca2-O9	2.349 (3)	2.556	2.541	2.528	2.356	2.338	2.317	2.572	2.578	2.593	2.350	2.310	2.282
Ca2-O4^{iii}	2.360 (2)	2.548	2.532	2.514	2.367	2.344	2.315	2.666	2.636	2.628	2.330	2.305	2.293
Ca2-O6	2.366 (3)	2.553	2.539	2.523	2.373	2.352	2.326	2.518	3.221	3.097	2.334	2.374	2.279
Ca2-O3^{iv}	2.447 (3)	2.608	2.586	2.566	2.477	2.463	2.422	3.312	2.950	2.916	2.453	2.419	2.469
Ca2-O11	2.457 (2)	2.618	2.578	2.554	2.485	2.449	2.414	3.209	2.614	2.588	2.398	2.345	2.388
Ca2-O2	2.472 (2)	2.614	2.599	2.581	2.497	2.475	2.455	2.675	3.456	3.369	2.414	2.383	2.387
Ca2-O14^{iii}	2.518 (3)	2.691	2.650	2.622	2.575	2.563	2.524	-	-	-	-	-	-
Ca3-O2^{v}	2.346 (3)	2.549	2.536	2.518	2.349	2.343	2.331	2.606	2.692	2.660	2.368	2.360	2.300
Ca3-O11	2.355 (3)	2.527	2.516	2.506	2.351	2.337	2.319	2.596	2.768	2.733	2.364	2.322	2.299
Ca3-O7^{v}	2.365 (2)	2.559	2.555	2.559	2.362	2.348	2.323	2.523	2.583	2.564	2.354	2.327	2.339
Ca3-O9	2.446 (2)	2.599	2.565	2.550	2.459	2.423	2.380	2.495	2.631	2.620	2.484	2.370	2.405
Ca3-O8	2.447 (3)	2.591	2.560	2.538	2.452	2.420	2.384	2.549	3.259	3.161	2.485	2.470	2.412
Ca3-O6^{v}	2.508 (3)	2.585	2.560	2.535	2.499	2.466	2.433	2.676	2.944	2.882	2.596	2.750	2.467
Ca3-O19	2.515 (3)	2.763	2.694	2.649	2.697	2.648	2.593	2.863	2.627	2.593	2.446	2.386	2.476
Ca4-O8^{vi}	2.348 (2)	2.547	2.533	2.524	2.358	2.339	2.311	2.584	2.705	2.671	2.367	2.314	2.337
Ca4-O1^{iv}	2.354 (3)	2.546	2.528	2.518	2.352	2.341	2.321	2.634	2.668	2.654	2.370	2.300	2.339
Ca4-O12	2.358 (3)	2.540	2.529	2.517	2.358	2.348	2.329	2.645	2.716	2.701	2.362	2.340	2.349
Ca4-O7	2.389 (2)	2.567	2.547	2.536	2.428	2.388	2.355	2.496	2.560	2.523	2.421	2.299	2.354

Ca4-O10	2.449 (3)	2.618	2.589	2.571	2.484	2.451	2.419	2.631	2.641	2.614	2.503	2.436	2.456
Ca4-O5^{vi}	2.464 (2)	2.589	2.570	2.546	2.473	2.460	2.440	2.572	2.516	2.494	2.551	2.387	2.445
Ca4-O15	2.553 (3)	2.683	2.637	2.616	2.614	2.573	2.537	2.619	2.545	2.513	2.493	4.443	2.392
Al1-O10^{vii}	1.897 (3)	1.854	1.840	1.826	1.929	1.913	1.896	1.855	1.831	1.821	1.938	2.064	1.922
Al1-O3^{viii}	1.901 (3)	1.861	1.851	1.849	1.921	1.919	1.908	1.966	1.854	1.850	1.952	1.926	1.925
Al1-O4^{v}	1.907 (3)	1.876	1.871	1.869	1.934	1.932	1.923	1.838	1.836	1.824	1.924	1.910	1.905
Al1-O2^{ix}	1.916 (3)	1.869	1.864	1.856	1.942	1.932	1.921	1.861	1.871	1.857	1.924	1.925	1.880
Al1-O9^{i}	1.918 (3)	1.872	1.857	1.848	1.935	1.923	1.910	1.794	1.785	1.780	1.935	1.826	1.917
Al1-O1^{iv}	1.923 (3)	1.879	1.876	1.867	1.951	1.940	1.931	1.886	1.921	1.914	1.945	1.942	1.921
Al2-O8	1.898 (3)	1.842	1.828	1.822	1.918	1.905	1.888	1.820	1.856	1.857	1.936	1.926	1.909
Al2-O7	1.899 (3)	1.856	1.849	1.847	1.924	1.914	1.901	1.829	1.854	1.840	1.903	1.903	1.888
Al2-O11	1.909 (3)	1.894	1.885	1.876	1.943	1.938	1.927	1.947	1.870	1.850	1.938	1.933	1.913
Al2-O12	1.917 (3)	1.875	1.866	1.853	1.931	1.920	1.907	1.937	1.887	1.887	1.938	1.904	1.925
Al2-O6	1.918 (3)	1.875	1.864	1.851	1.948	1.940	1.929	1.857	1.815	1.808	1.946	1.973	1.900
Al2-O5	1.925 (3)	1.880	1.873	1.863	1.947	1.942	1.933	1.896	1.821	1.807	1.948	1.954	1.941
O18-C1	1.283 (3)	1.293	1.291	1.289	1.304	1.302	1.299	1.305	1.323	1.324	1.379	1.303	1.369
O19-C1^{v}	1.299 (4)	1.299	1.296	1.295	1.308	1.305	1.302	1.283	1.286	1.283	1.276	1.298	1.274
O20-C1	1.284 (3)	1.271	1.270	1.268	1.295	1.291	1.289	1.288	1.274	1.272	1.267	1.305	1.271
H13A-O13-H13B	98 (2)	109.7	109.9	109.5	106.4	106.5	106.2	107.2	94.5	94.0	103.7	132.1	101.2
O18-C1-O20	120.2 (2)	121.1	121.4	121.7	120.6	120.7	120.7	118.9	118.2	118.1	115.9	120.7	115.5
O18-C1-O19^{vi}	120.2 (2)	118.7	118.4	118.2	119.6	119.4	119.3	118.7	119.0	118.6	117.4	119.44	118.0
O20-C1-O19^{vi}	119.6 (3)	120.2	120.2	120.0	119.7	119.9	120.0	122.3	122.4	122.7	126.8	119.8	126.5

Note: Experimental data is from (François et al., 1998). Symmetry codes: (i) x,y-1,z; (ii) x,y,1+z; (iii) x,1+y,z; (iv) x,y,z-1; (v) x-1,y,z; (vi) 1+x,y,z; (vii) x-1,y,z-1; (viii) x,y-1,z-1; (ix) x-1,y-1,z.

SUPPLEMENTARY TABLE 2. Hydrogen-bonding geometry (Å, °).

	$C_4AC_2H_{11}$							$C_4AC_2H_8$					
	Exp	LDA			GGA			LDA			GGA		
P (GPa)	0.0	0.0	2.0	5.0	0.0	2.0	5.0	0.0	2.0	5.0	0.0	2.0	5.0
$O17^{i}$-$H17B^{i}$	0.82 (3)	1.03	1.04	1.04	1.01	1.01	1.02	-	-	-	-	-	-
$O15^{iv}$-$H15B^{iv}$	0.92 (2)	1.05	1.05	1.05	1.02	1.02	1.02	1.01	1.00	1.00	1.47	1.22	1.37
$O16^{iv}$-$H16A^{iv}$	0.97 (3)	1.00	1.00	1.00	0.99	0.99	0.99	-	-	-	-	-	-
$O16^{iv}$-$H16B^{iv}$	0.95 (3)	1.02	1.02	1.02	1.01	1.01	1.01	-	-	-	-	-	-
O14-H14A	0.92 (3)	1.02	1.02	1.02	1.00	1.01	1.01	-	-	-	-	-	-
O14-H14B	0.90 (4)	1.04	1.04	1.04	1.02	1.02	1.02	-	-	-	-	-	-
$H17B^{i}$-O14	1.85 (3)	1.55	1.51	1.48	1.67	1.62	1.57	7.82	7.54	7.46	8.28	8.00	7.69
$H15B^{iv}$-O18	1.71 (2)	1.47	1.47	1.46	1.59	1.58	1.56	1.73	1.82	1.79	1.07	5.85	1.10
$H16A^{iv}$-O18	1.79 (3)	1.73	1.70	1.68	1.78	1.74	1.71	12.75	14.04	13.85	13.29	13.78	12.73
$H16B^{iv}$-O19	1.75 (3)	1.57	1.56	1.54	1.64	1.61	1.59	12.12	12.73	12.59	12.91	13.40	12.25
H14A-O19	1.86 (3)	1.58	1.55	1.52	1.72	1.66	1.62	3.73	3.55	3.52	4.38	4.49	3.88
H14B-O20	1.74 (4)	1.52	1.49	1.46	1.61	1.59	1.56	5.90	6.80	6.70	6.68	6.79	6.05
$O17^{i}$-O14	2.746 (4)	2.580	2.547	2.521	2.675	2.631	2.586	7.820	7.541	7.458	8.284	8.002	7.692
$O15^{iv}$-O18	2.631 (4)	2.514	2.505	2.499	2.607	2.594	2.573	2.725	2.821	2.791	2.529	5.617	2.458
$O16^{iv}$-O18	2.750 (4)	2.727	2.700	2.679	2.771	2.724	2.690	12.745	14.043	13.848	13.293	13.779	12.729
$O16^{iv}$-O19	2.681 (4)	2.585	2.569	2.550	2.645	2.614	2.585	12.117	12.734	12.587	12.905	13.396	12.253
O14-O19	2.774 (4)	2.605	2.568	2.540	2.726	2.665	2.623	3.729	3.554	3.524	4.381	4.491	3.877
O14-O20	2.626 (4)	2.553	2.523	2.499	2.633	2.608	2.577	5.898	6.799	6.696	6.677	6.794	6.051
$O17^{i}$-$H17B^{i}$-O14	163 (3)	175	175	175	174	175	176	-	-	-	-	-	-
$O15^{iv}$-$H15B^{iv}$-O18	171 (3)	170	169	168	171	171	170	169	177	176	173	73	170
$O16^{iv}$-$H16A^{iv}$-O18	165 (5)	175	175	174	177	175	173	-	-	-	-	-	-
$O16^{iv}$-$H16B^{iv}$-O19	165 (4)	171	170	170	170	168	167	-	-	-	-	-	-
O14-H14A-O19	173 (3)	178	177	177	175	174	173	-	-	-	-	-	-
O14-H14B-O20	171 (4)	171	172	172	175	175	176	-	-	-	-	-	-

Note: Experimental data is from (François et al., 1998). Symmetry codes: (i) x,y-1,z; (iv) x,y,z-1.

480
481 **FIGURES**
482

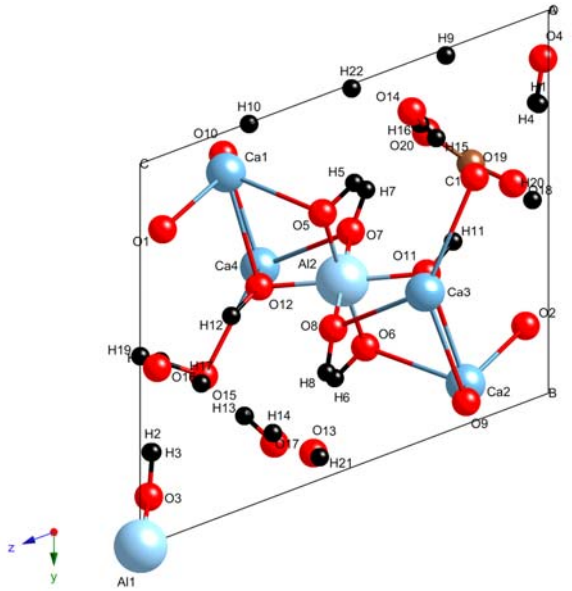

483
484 **Figure 1.**

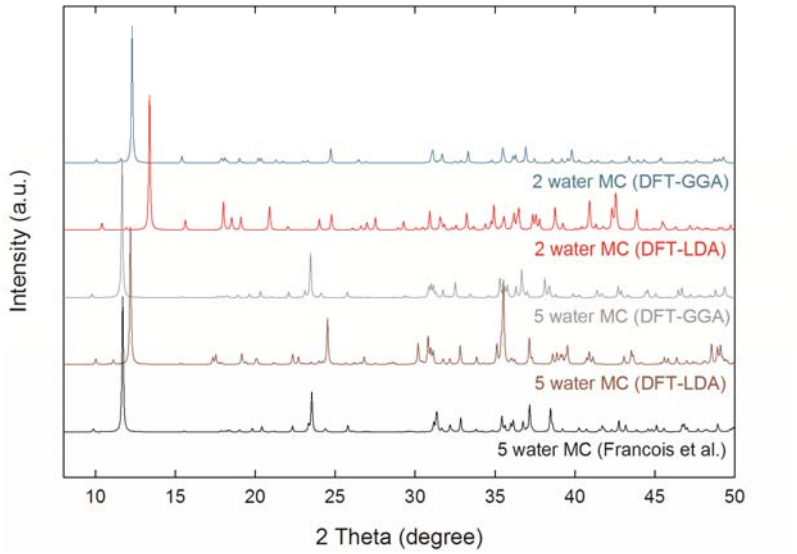

485
486 **Figure 2.**

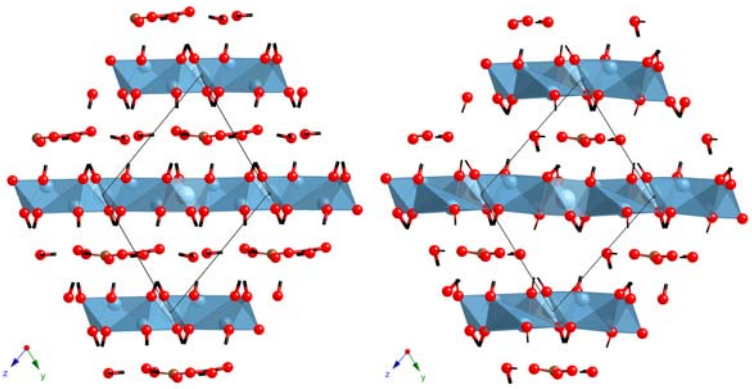

Figure 3 (left and right)

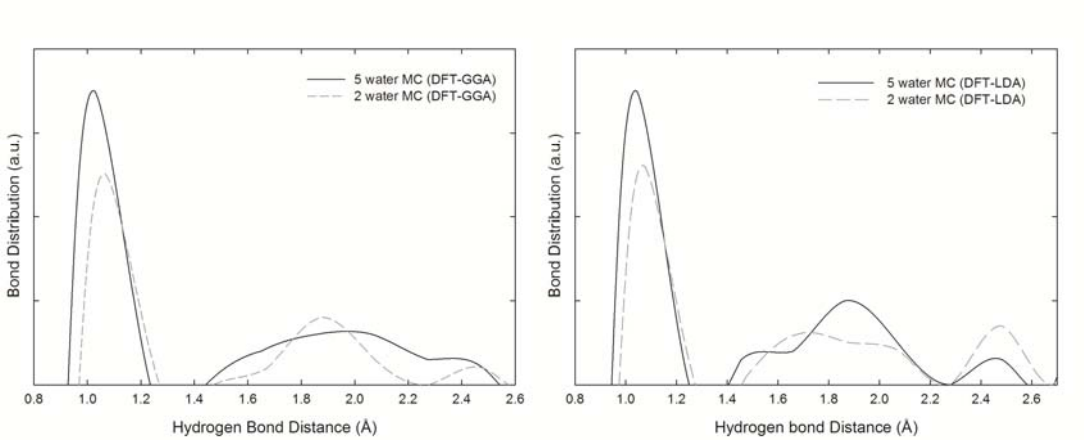

Figure 4 (left and right)

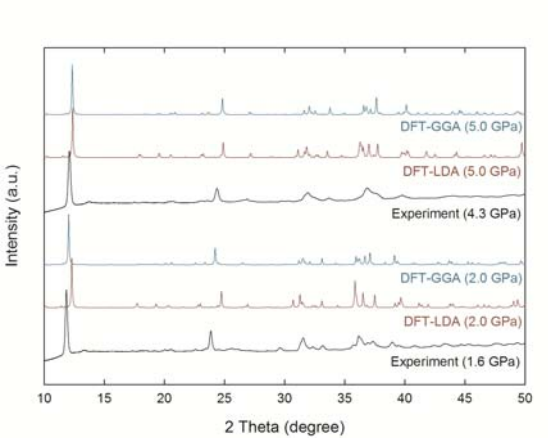

Figure 5

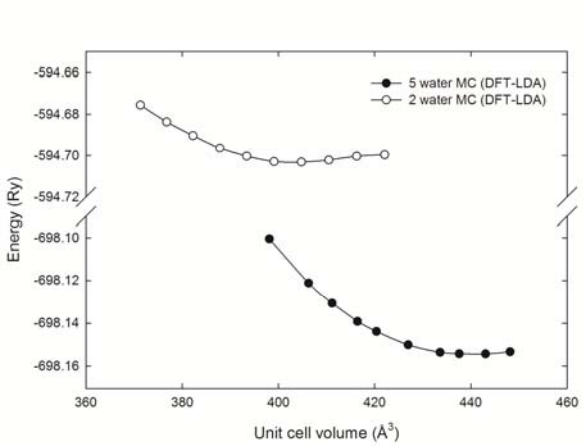

Figure 6

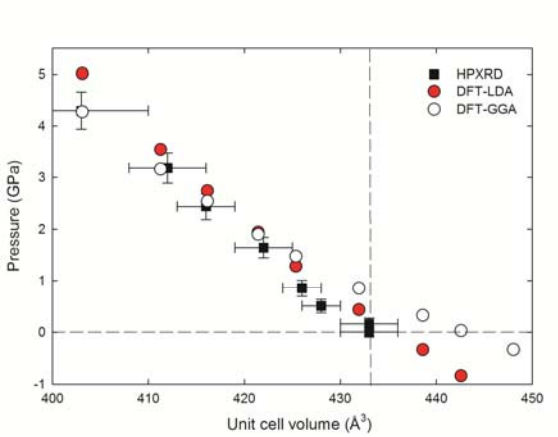

Figure 7

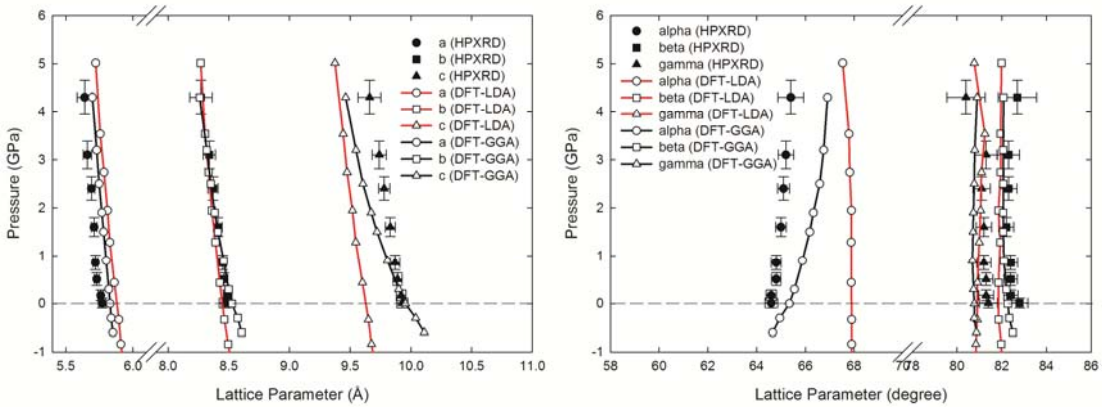

Figure 8 (left and right)

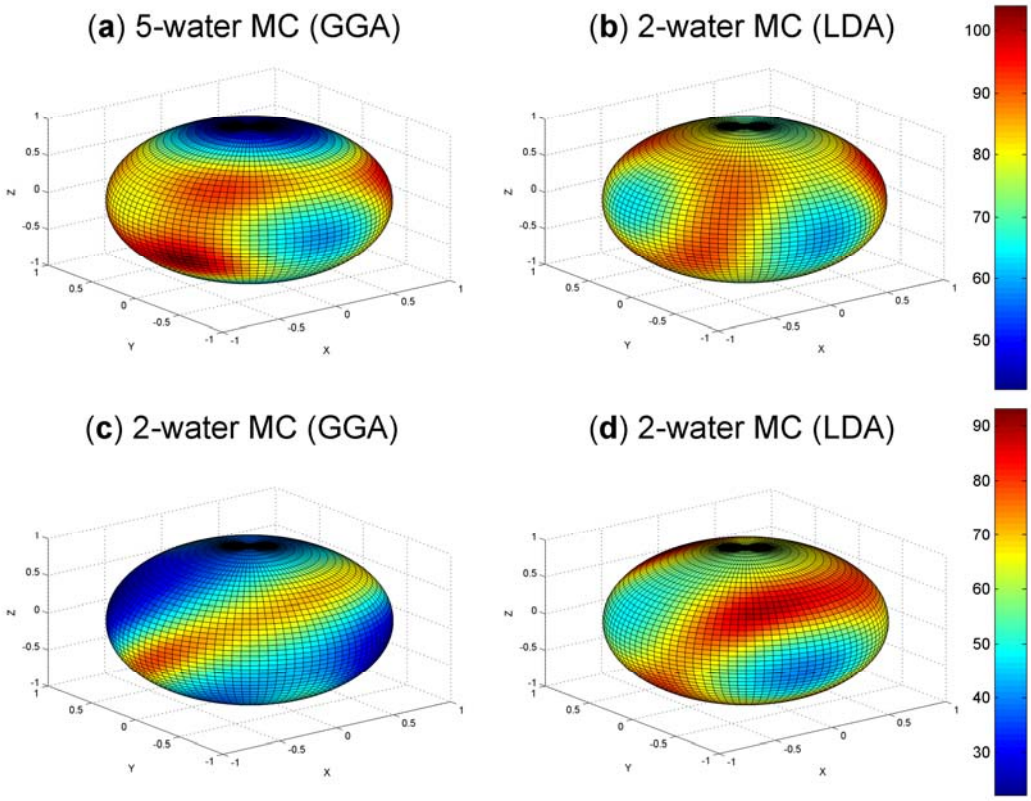

Figure 9

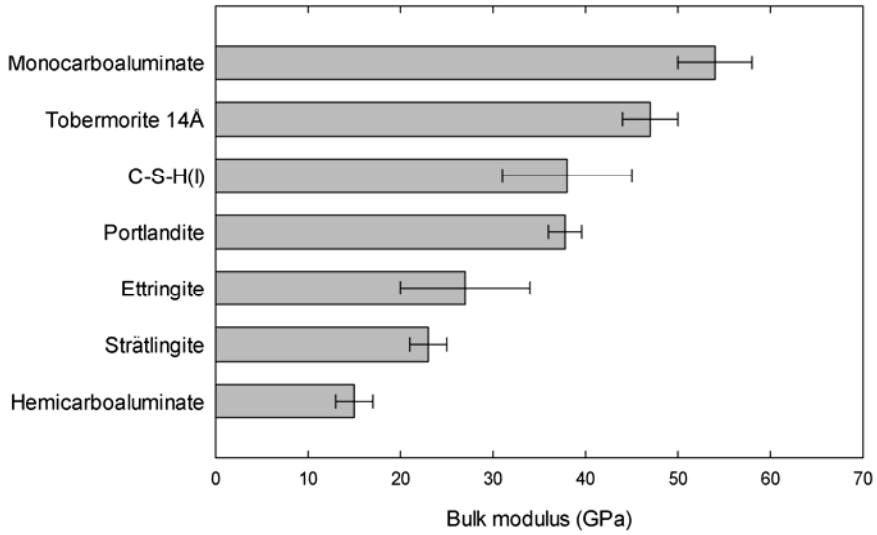

Figure 10